



Lattice Boltzmann simulations in a rectilinear cascade configuration for the turbulence-airfoil interaction noise evaluation and reduction through serrated leading edges

Martin Buszyk¹, Thomas le Garrec¹, Cyril Polacsek¹, Raphaël Barrier²

¹DAAA, ONERA, Université Paris-Saclay, 92320 - Châtillon, France
martin.buszyk@onera.fr, thomas.le_garrec@onera.fr, cyril.polacsek@onera.fr

²DAAA, ONERA, Université Paris-Saclay, 92190 - Meudon, France
raphael.barrier@onera.fr

Abstract

The turbulence-airfoil interaction mechanism is a dominant source of turbofan noise. A low-noise design based on leading edge serrations is proposed and will be tested in a rectilinear cascade configuration. Performances are assessed by numerical simulations and analytical approach. A first numerical methodology based on linearized Euler equations coupled with a synthetic turbulence generation process has been investigated. In this paper, the attention is paid on high-fidelity simulations using the Lattice Boltzmann method with the ProLB software. It allows to capture the actual turbulent flow on the full cascade rig including the turbulence grid and to perform direct acoustics, with an easy and fast numerical setup resulting from the combination of octree meshes and immersed boundary conditions. First simulations are focused on the baseline geometry which is a major step before trying to assess the noise reduction from the serrated design. Relevant aerodynamic and acoustic fields are post-processed and discussed through comparisons with RANS solutions and CAA predictions previously obtained, waiting for test campaign and experimental data.

Keywords: aeroacoustics, lattice Boltzmann method, turbulence-cascade interaction, grid turbulence.

1 Introduction

To design future green aeroengines, additional effort is needed to reduce the tonal and broadband noise components to comply with tightening regulations. The major contribution behind dominant aeroacoustic sources is the rotor-stator interaction noise, particularly at approach condition. In this purpose, a European project InnoSTAT (Innovative stators) has been launched in 2019 in order to investigate promising low noise designs to be applied to the stator vanes. A laboratory test campaign will be conducted at Ecole Centrale de Lyon (ECL) facility on a rectilinear cascade impinged by a roughly isotropic turbulent inflow generated by an adequately shaped turbulence grid. ONERA is contributing to the project by proposing a state-of-the-art passive treatment based on current leading edge serrations, which concept has intensively been studied in recent works [1-6]. This design contribution is associated with numerical simulations and analytical predictions of the expected broadband noise radiation and reduction obtained with the baseline (untreated) and serrated designs, with a checking of aerodynamic performances too. On the numerical side, a practical alternative to costly LES methods currently adopted for aeroacoustic computations relies on CAA by solving the linearized Euler equations [1-3,7]. This propagation simulation related to the disturbance fields, requires a prescribed convection mean flow obtained from a CFD (RANS or Euler) solver and above all a representative synthetic turbulent flow to be injected at the entrance of the CAA domain. In previous studies, ONERA has used a Stochastic Noise Generation and Radiation (SNGR) framework to this end [1-3,7]. In recent years, high-fidelity approach based on lattice Boltzmann equations has shown to be a serious competitor. In fact, through

the full immersed boundary conditions (IBC) and octree-mesh resolution, its low dissipative effects and very fast computing ability allow to simultaneously assess the turbulent flow and direct acoustic field in very complex configurations. Therefore, contrary to hybrid CAA computations performed on a limited domain and requiring a synthesized turbulence beforehand, the LBM simulation presented in this paper considers the overall ECL test rig including the turbulence grid. ONERA computations are performed with the ProLB code, which has shown to be relevant for similar configurations [8]. In the literature, some numerical studies have also been conducted using the well-known code Powerflow. One of these studies [4], focused on a realistic turbofan stage equipped with serrated vanes. However, observed noise reduction was found to be small due to a non-suited choice of the serration parameters (amplitude-to-wavelength ratio much lower than 1). Teruna et al. have investigated the rod-airfoil noise [5] along with the effect of both porosity and serrations on noise [6], achieving a significant reduction on pure tones and broadened tones. The aim of our numerical study relying on LBM is to highlight the expected noise reduction from serrations designed by ONERA over a relevant broadband range, while keeping aerodynamic penalties as low as possible. The simulations are restricted to the approach operating point due to Mach limitation of the numerical scheme ($M < 0.7$). In section 2, the test facility will be described. Model behind the ProLB code, used for the LBM calculations, is briefly presented in section 3 along with the methodology used for acoustic post-treatments. First computations on a coarse mesh are then performed and analysed in section 4 mainly to adjust the set-up conditions, in order to assess the target mass flow. Computations are then extended on a medium mesh so that the properties of the turbulence grid can be analysed, as well as far-field SPL spectra, these ones being obtained either directly or from an integral method. Results are then compared to RANS and CAA computations [3]. In last section 5, the numerical set-up with the serrated geometry is presented.

2 Experimental set-up

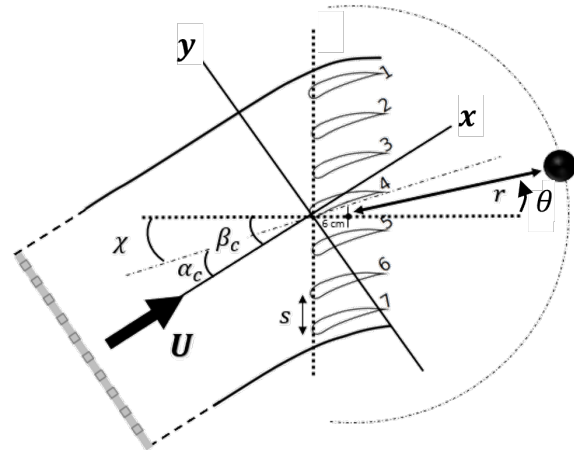
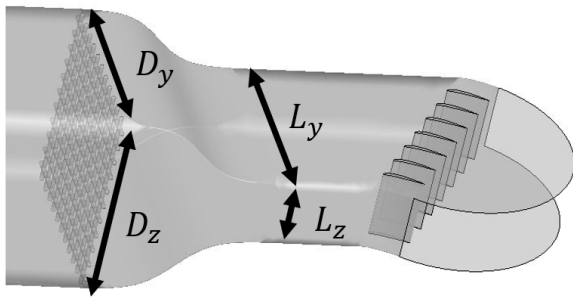


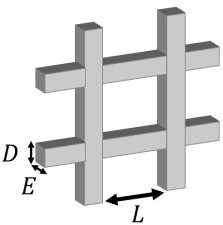
Figure 1 – 3D view (mesh) of the test facility.

Figure 2 – Top view (sketch) of the test facility.

In the framework of the InnoSTAT project, several noise reduction technologies will be evaluated during a laboratory test campaign. The ECL test facility consists in a rectilinear cascade of seven evenly spaced NACA7310 airfoils placed in a rectangular test section [9]. The cascade is impinged by a turbulent flow generated by a turbulence grid placed upstream of the nozzle as illustrated in Fig. 1 and Fig. 2. The nozzle squeezes the flow to obtain higher mean velocity in the vicinity of the cascade. The dotted half-circle in Fig. 2 represents the far-field microphone antenna located at $r = 1.88$ m from the cascade plane centre. The parameters used for the LBM computation are summarized in Table 1. The target values are derived from Safran specifications, roughly adapted from a specific turbofan at approach operating point (OP). Although, these pre-test values are not definitive, they should remain closed to the final ones. The proposed turbulence

grid has been previously evaluated in another test rig [10], achieving a turbulent intensity (TI) of 4.5 % and an integral length scale ($L_{11,1}$ in Eq.s (2) and (3)) of 9 mm, both quantities probed at 50 cm from the grid.

Table 1 – Parameters used for the LBM computations.

Test-section geometry	$(D_y, D_z)=(56 \text{ cm}, 56 \text{ cm})$ and $(L_y, L_z)=(56 \text{ cm}, 20 \text{ cm})$	
Turbulence grid		$D = 1 \text{ cm}$ $E = 1 \text{ cm}$ $L = 4 \text{ cm}$
Mean flow	Mach (in front of the cascade)	0.34
Airfoils – NACA7310	Chord c	12 cm
	Span L_z	20 cm
	Inter-vane spacing	8.5 cm
	Angles $(\alpha_c, \beta_c, \chi)$	$(20^\circ, 34^\circ, 14^\circ)$

3 Brief overview of the LBM solver

LBM simulations are performed using the ProLB solver developed in the framework of a French consortium composed of universities, research institutes and industries (<http://www.prolb-cfd.com/>). A D3Q19 lattice, illustrated in Fig. 3, is used to compute the distribution function. As for the numerical scheme, a Hybrid Recursive Regularized approach is used [11]. It includes some corrections to cancel $O(M^3)$ terms leading to a more robust code under $M=0.7$, while remaining athermal. As for the turbulence, a shear-improved Smagorinsky model [12] is used here. Near solid surfaces defined by means of immersed boundary conditions, the fluid boundary layer is resolved thanks to an advanced wall log-law which takes into account adverse pressure gradient and curvature effect. As detailed later in the numerical set-up, direct acoustic computations are performed and extracted using probes suitably placed in the numerical domain, corresponding to the microphone antenna to be used during the test campaign (Fig. 2). Wall pressure is also extracted on the vane skin aiming to perform an indirect computation of the radiated far-field noise, using the in-house tool, MIA which solves Kirchhoff integral in the frequency domain.

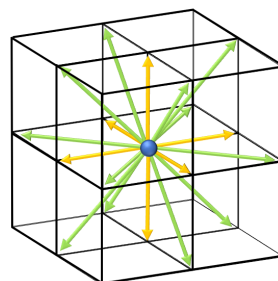


Figure 3 – Illustration of the discrete velocities in a D3Q19 lattice.

4 Computations performed on the baseline (untreated) geometry

4.1 Coarse mesh set-up and preliminary solutions

First calculations are performed on a coarse mesh in order to check the numerical set-up and to adjust the input conditions. The global 3D domain mesh is illustrated in Fig. 4, indicating the different grid resolutions. It consists of 140 million points or 24 million fine equivalent points. The far-field condition is set to the atmospheric pressure. At the entrance of the domain, a uniform velocity condition is imposed. In this region, a slip boundary condition is used at the walls of the test section. Then, a solid wall condition is applied inside the test section as well as on the skin of turbulence grid and vanes. An overall simulation time $T_{sim} \approx 0.404$ s is considered, which is reached after 300,000 timesteps, ensuring a good convergence of the averaged solution (see Fig. 5). A probe is placed half a chord upstream of the leading edge of the central vane in order to monitor the mean flow. Few iterations are needed to adjust the input velocity to obtain a value of the Mach number closed to the targeted one. The evolution of the convergence process is clearly shown in Fig. 5.

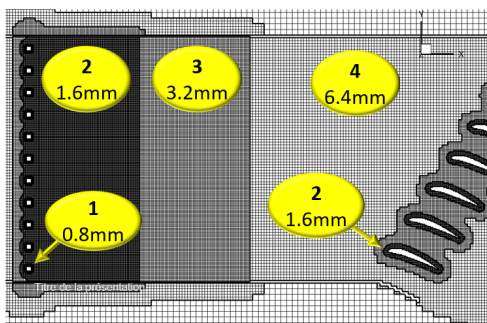


Figure 4 – Refinement levels of the coarse mesh.

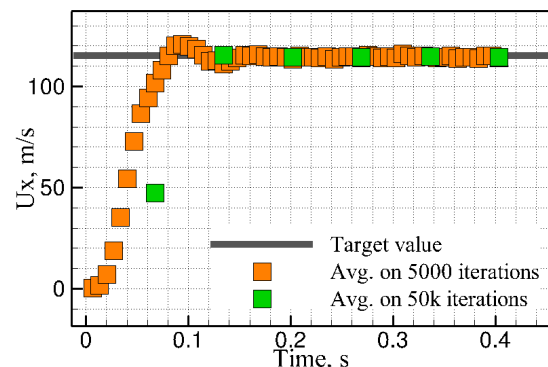


Figure 5 – Averaged (mean) axial flow velocity, $\frac{1}{2}$ chord upstream of the central leading edge.

Preliminary results obtained from the coarse mesh set-up are a guidance for the definition of the refined (so-called medium in the paper) mesh set-up which is presented in the following section.

4.2 Computations on a “medium” mesh to assess turbulence and acoustics

4.2.1 Medium mesh set-up

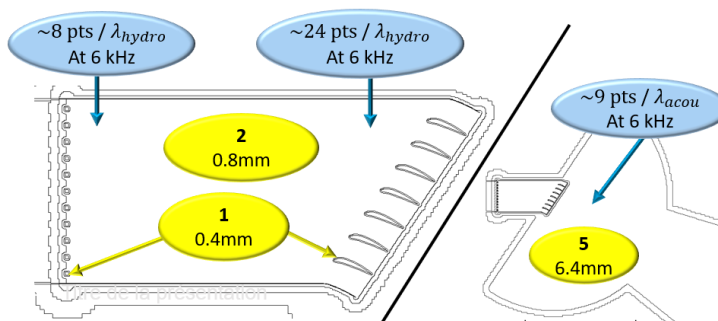


Figure 6 – Refinement levels of the “medium” mesh. Number of points per wavelength for a 6 kHz wavelength.

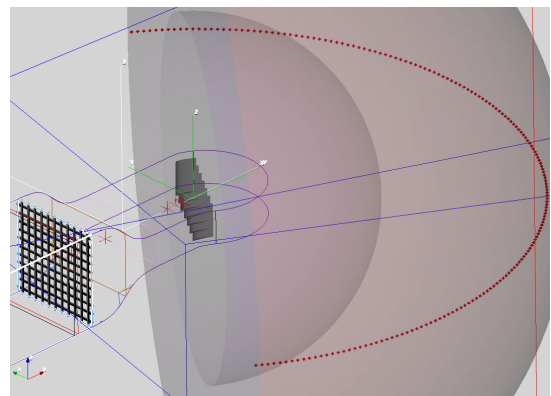


Figure 7 – Simulation domain in ProLB interface. Microphones antenna is represented by red dots.

The near wall mesh must be refined to get an y^+ in a range lower than 300, where the wall law is well defined. This is achieved on the "medium mesh configuration", for which the smallest mesh size has been divided by two: $\Delta_{x_{min}} = 0.4$ mm, which lead to a mesh of 940 million points or 260 million fine equivalent points. The calculation is performed on 600,000 iterations and keeping $T_{sim} \approx 0.404$ s. This set-up should allow to accurately capture the turbulence characteristics beyond the grid, while ensuring well resolved acoustic predictions up to at least 6 kHz. Mesh densities are illustrated in Fig. 6. Contrary to the coarse case, there is no transition in the mesh densities between the grid and the airfoils to avoid possible discontinuities in the turbulent flow convection. Moreover, an acoustic zone (half sphere) has been added has shown in Fig. 7 to perform direct acoustic predictions. In first instance, the y^+ distribution is checked as illustrated in Fig. 8a and Fig. 8b. On both grid and vane walls, it is now in the desired range, contrary to the coarse mesh case.

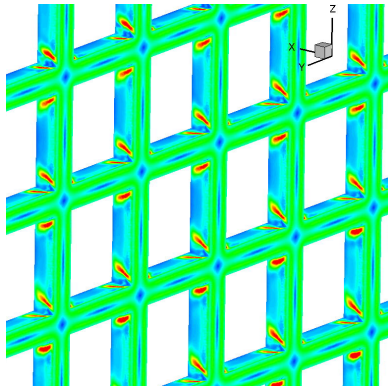


Figure 8a – Averaged (over 100k iterations) y^+ distribution (level between 0 and 50).

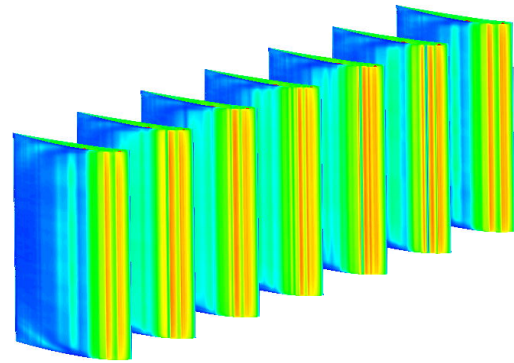


Figure 8b – Averaged (over 100k iterations) y^+ distribution (level between 0 and 200).

4.2.2 Turbulent flow analyses

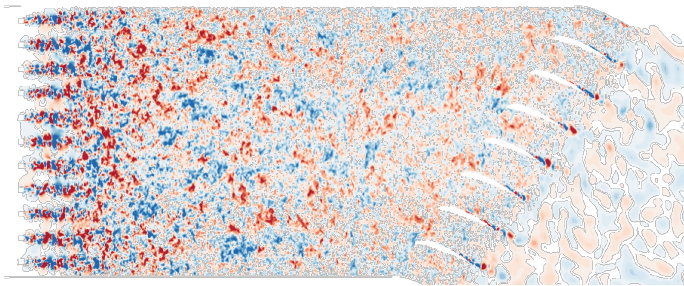


Figure 9 – u'_y velocity field (level between ± 10 m/s). Cut view in the $(x, y, z=0)$ plane.

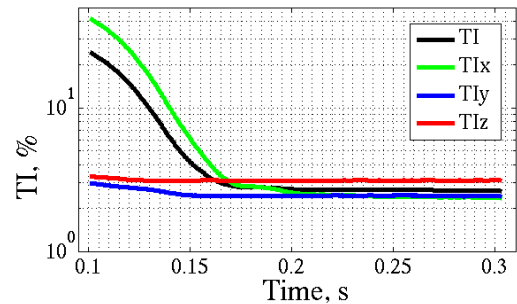


Figure 10 – Time evolution of TI, obtained on a moving interval of width $T_{sim}/2$.

The evolution of the turbulence beyond the grid, depicted in Fig. 9, is analysed in this section. On this colormap, the turbulent structures generated by the grid and convected up to the cascade are found to be homogeneously distributed without noticeable discontinuities nor dissipation effects.

$$TI = \frac{\sqrt{1/3 (\overline{u_1'^2} + \overline{u_2'^2} + \overline{u_3'^2})}}{U_1} \quad \text{and} \quad TI_i = \frac{\sqrt{\overline{u_i'^2}}}{U_1} \quad (1)$$

The turbulent intensity (TI) with respective contribution along each direction is obtained from Eq. (1).

$$L_{ii,k}(\mathbf{X}) = \int_0^R \frac{\overline{u'_i(\mathbf{X} - \mathbf{r}_k, t)u'_i(\mathbf{X} + \mathbf{r}_k, t)}}{\sqrt{\overline{u'_i(\mathbf{X} - \mathbf{r}_k, t)u'_i(\mathbf{X} - \mathbf{r}_k, t)}}\sqrt{\overline{u'_i(\mathbf{X} + \mathbf{r}_k, t)u'_i(\mathbf{X} + \mathbf{r}_k, t)}}} dr_k \quad (2)$$

$$L_{11,1} = \frac{S_{11}(f=0)U_1}{2\overline{u_1'^2}} \quad (3)$$

The integral length scale ($L_{11,1}$), is computed using the autocorrelation function following Eq. (2). This turbulent length scale is also estimated by using the usual approximation of Eq. (3) related to the PSD (power spectrum density) of the streamwise velocity component, S_{11} .

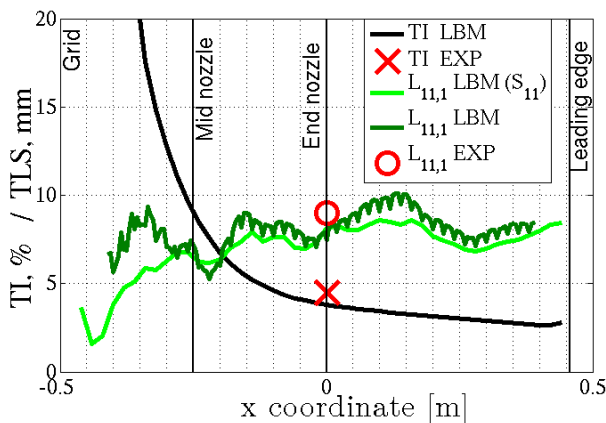


Figure 11 – Axial evolution of the TI and integral length scale in the test section. Values obtained on the interval $[T_{sim}/2, T_{sim}]$.

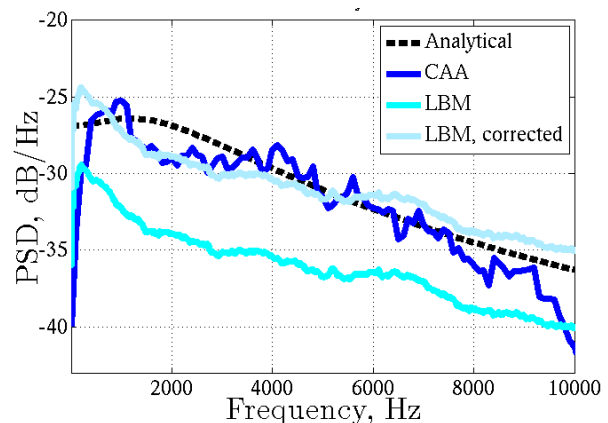


Figure 12 – PSD of the upwash velocity fluctuations near the LE. Corrected value shifted by a factor $10 \log \left(\frac{TI_{CAA}}{TI_{LBM}} \right)$. 1 kHz moving averaged applied.

The time evolution of the turbulence intensity close to the leading edge is plotted in Fig. 10, showing a very good convergence from $t \approx 0.2$ s after a transient period, and a roughly isotropic trend despite an amplification of the z-component, which might be due to the fact that the contraction of the test section is very strong (ratio 2.8) and only on this z-direction. The spatial evolution of the turbulent properties is plotted in Fig. 11. Experimental target values at 50 cm from the grid (although obtained on a different set-up [10]), are also indicated with red symbols. A quite good agreement is observed, regardless the estimation process for TLS (Eq.s (2) or (3)). This LBM analysis with respect to the turbulence grid properties is then successful. Near leading edge PSD of the upwash velocity component is compared to CAA calculation [3] in Fig. 12, showing a small difference in slopes at high frequencies.

4.2.3 Basic aerodynamics and comparisons with RANS

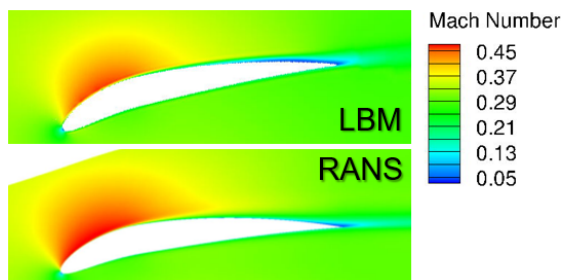


Figure 13 – Mach number fields from LBM and RANS [3] computations.

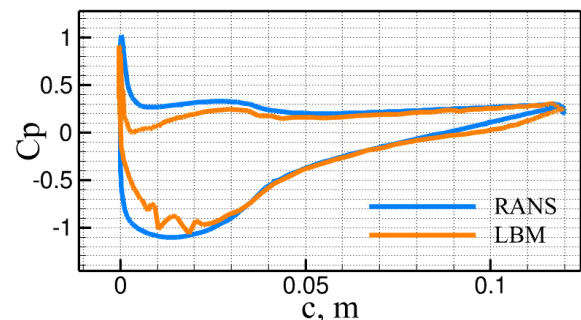


Figure 14 – Wall pressure coefficient from LBM and RANS [3] calculations.

First RANS calculations have been performed on the baseline (untreated) geometry [3]. A one-channel domain with periodic boundary conditions has been considered. For these computations, angles were slightly different $(\alpha_c, \beta_c, \chi) = (24^\circ, 33^\circ, 9^\circ)$, since the geometry was defined before the final pre-test value (in Table 1) were provided. Fig. 13 illustrates the mean velocity field provided by RANS and LBM computations, where a small difference appears in the boundary layer near trailing edge (suction side). The pressure coefficient is plotted in Fig. 14. Although differences which might be link to the difference in angle values appear, results remain closed between the two methods.

4.2.4 Acoustic analyses and comparisons with CAA

First of all, the RMS (root mean square) wall pressure over the vane surface is discussed. A comparison is performed with a previous CAA computation [3], which has consisted in a 3-vanes domain with periodic conditions and a 3D synthetic turbulence based on the Liepmann spectrum model calibrated with slightly different pre-test values: $TI = 5\%$ and $L_{11,1} = 8\text{ mm}$. Figs 15 and 16 show the RMS wall pressure on the vane suction side from the CAA and LBM calculations, respectively. For the CAA, there is no pressure at the corners of the leading edges because of the windowing of the synthetic turbulence injection [3], and the sources are only concentrated in the leading-edge region. These leading-edge sources are also clearly visible in the LBM solution, but intense spots are present near the trailing edge. These additional sources might be linked to laminar-turbulent transition in the boundary layer in this area (see section 4.2.3) and not present in the CAA since the mean flow was obtained using an Euler code.

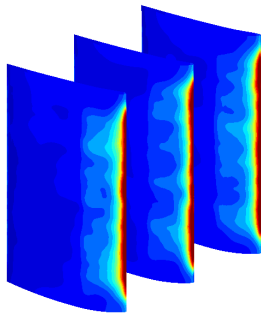


Figure 15 – p'_{RMS} on vane suction side (levels between 0 and 500 Pa) from CAA calculation [3].

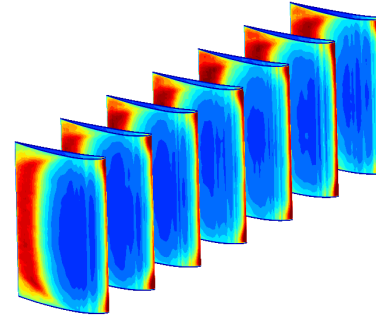


Figure 16 – p'_{RMS} on vane suction side (levels between 0 and 500 Pa) from LBM calculation.

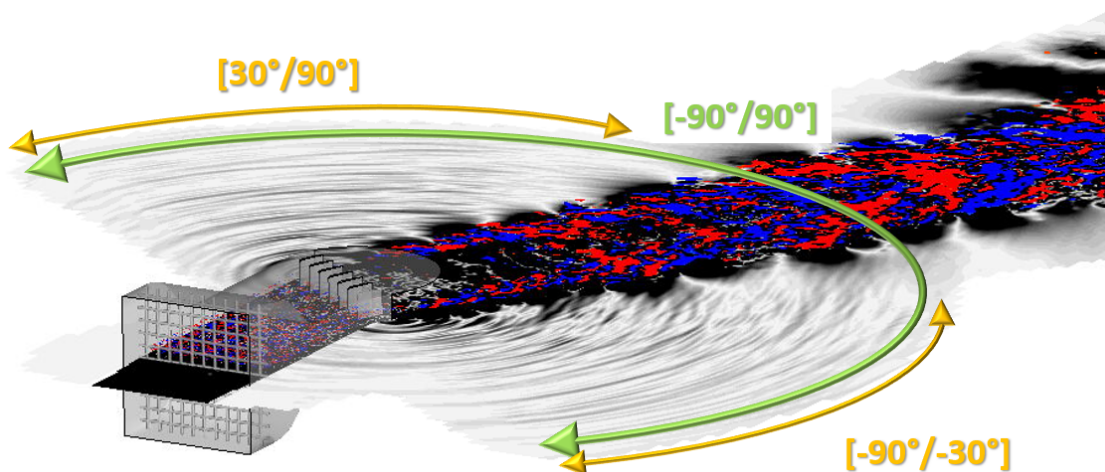


Figure 17 – Snapshot of $|p'|$ (0 to 20 Pa) and $|u'_z|$ (± 4 to ± 6 m/s)

The following analyses are devoted to the radiated sound field. In Fig. 17 a snapshot of the fluctuating pressure field and turbulent wake downstream of the cascade exhaust can be visualized. The wake generates strong

pressure fluctuations, polluting the direct acoustic extractions and probably the acoustic measurements from the microphone antenna, so that the exploitable region is restricted to the split arcs plotted in orange. Outside of the wake region, the acoustic waves radiating in the far-field are clearly visible. Concerning the acoustic post-processing, the two methodologies previously discussed, relying on the Ffowcs Williams-Hawkings (FWH) analogy and on direct acoustics, are investigated. First, the reward sound power spectrum is computed thanks to the integral method (using the code MIA). The unsteady pressure on the vane surface is extracted and stored throughout the simulation time. Then, a Fourier transform is applied (with $\Delta f \approx 5\text{Hz}$) to provide the harmonic loadings used as inputs in MIA solving the FWH integral restricted to the loading noise term (largely dominant contribution). Hence, the radiated sound field is obtained by considering a flow at rest. The sound power level is computed for probes located at $R_{obs} = 1.88\text{ m}$ from the centre of the cascade. Two angular integrations are considered for the microphones: $[-90/90^\circ]$ and $[-90/-30^\circ] \cup [30/90^\circ]$ (to avoid hydrodynamic fluctuations in the wake for the direct calculation method as illustrated by Fig. 17). The sound power radiated downstream is estimated using the approximation already used in [2-3] and written as (with S_{pp} , the acoustic pressure PSD):

$$\text{PWL} = 10 \log \left(\frac{\int_{\theta} \frac{r L_z}{\rho_0 c_0} S_{pp} d\theta}{W_{ref}} \right), W_{ref} = 10^{-12} \text{W} \quad (4)$$

The convergence of the far-field acoustics is assessed in Fig. 18, where the SPL (sound pressure level) is probed at one location ($\theta = 90^\circ$). Only a small transient time ($T_{sim} = 1/6$) is visible. As for the radiated sound downstream of the cascade, there is a good agreement between the direct and indirect calculations as shown in Fig. 19, up to 6 kHz where the acoustic waves start to be dissipated by the LBM grid. For comparison purposes the spectrum issued from the CAA computation has been added [3]. The direct and indirect LBM solutions are quite close when the wake is excluded from the integral of Eq. (4) and responsible for a strong increase of the levels in the low and medium frequency range. The grid cut-off is clearly visible beyond 6.5 kHz, which as expected based on the mesh design explains the slope deviation by comparing with the LBM direct spectrum. The LBM+FWH spectrum is not far from the CAA solution up to 5 kHz, showing a higher attenuation slope. These deviations might be attributed to different turbulent inflow characteristics at the leading edge plane in the CAA and LBM simulations. Noise sources have also been integrated on 50% of chord (suction side) near the trailing edge (TE) as illustrated on Fig. 19. Even if their contribution is not negligible, they do not represent the dominant source of noise, as it could have been forecast from Fig. 16.

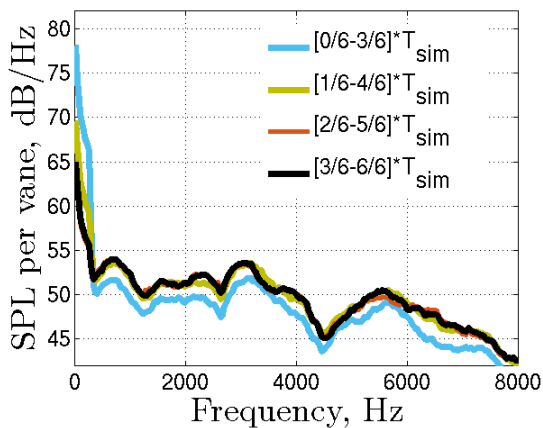


Figure 18 – SPL level at $r = 1.88\text{ m}$ and $\theta = 90^\circ$, for different sliding periods. A 1 kHz moving averaged has been applied.

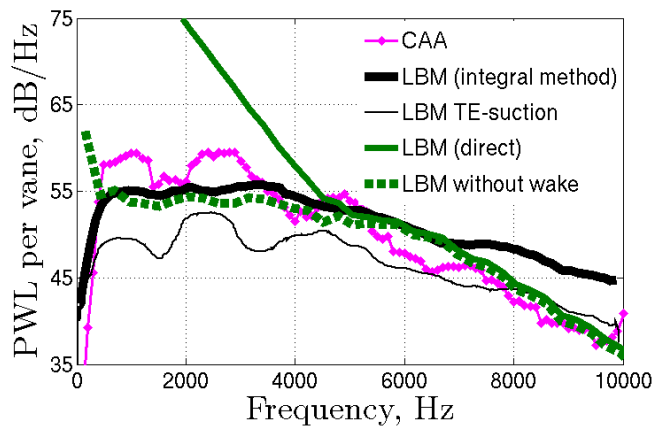


Figure 19 – Downstream radiated power spectra (at $r = 1.88\text{ m}$). LBM spectra computed on the last period $[T_{sim}/2, T_{sim}]$. A 1 kHz moving averaged has been applied.

5 Low-noise geometry set-up

The next LBM set-up with serrated vanes (still undergoing) is briefly discussed in this last section. The low-noise geometry design has been defined accordingly to previous studies [1-3,7] and CFD (RANS) and CAA calculations have been already performed on this treated case [3]. The leading-edge shape has been defined based on the turbulence length scale with $\lambda_s = 16,7$ mm (12 patterns along the span) which matches approximately four times the transversal length scale ($L_{22,3} = 1/2L_{11,1}$), for an isotropic turbulence), while setting the amplitude of the serration so as $h_s/\lambda_s = 1$. These values are also ensuring a "good-practice" criterion ($h_s < 0.15c$) aiming at limiting the aerodynamic penalties, as mentioned in [1]. The 3D shape has been obtained from the 2D design (Fig. 20) thanks to an in-house modeller, ersatzZ [3]. The 3D geometry of the 7-vanes cascade with leading edge serrations to be used in the new LBM set-up is shown in Fig. 21.

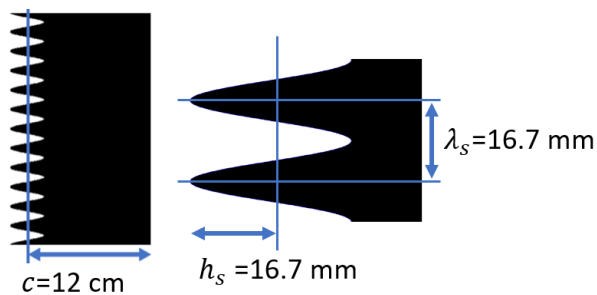


Figure 20 – 2D geometry of the serrated design.

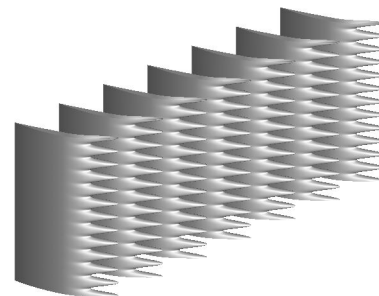


Figure 21 – Rectilinear cascade of NACA7310 airfoils with serrated leading edge.

6 Conclusion

Numerical simulations with the LBM code ProLB have been performed in order to assess the aeroacoustic response of a rectilinear cascade impinged by a turbulent inflow generated by a turbulence grid. The LBM capability allows to consider the complete test facility (at Ecole Centrale de Lyon) in the numerical set-up, which is the first experimental campaign scheduled in the InnoSTAT project. The present study has been focused on the baseline case, to be used as a reference before evaluating the acoustic performances of a low-noise treatment (serrated vanes). A first bench of computations has been performed on a coarse mesh to adjust the adequate input conditions at the entrance of the test section and to match the target values (in terms of flow angle and Mach number). Then, computations have been conducted on a medium mesh. Turbulence properties generated by the turbulence grid have been first analysed and favourably compared with available target values from previous tests, even if the influence of the strong nozzle contraction has been emphasized. A satisfactory agreement has been obtained when comparing the basic aerodynamics from LBM to the RANS solutions, although a 4 deg. deviation for stagger angle in the respective set-up (earlier pre-test value adopted in the RANS) was reported. Finally, acoustic predictions in terms of SPL and PWL spectra have been performed using both indirect (chaining LBM with FWH analogy to radiate the vane loadings) and direct (LBM sound field extraction from far-field probes) methodologies, showing a very good agreement up to the expected cut-off frequency (6-7 kHz) of the medium mesh. A comparison with a previous CAA solution has been realized too. A reasonable agreement has been found, but a stronger attenuation slope is observed in the CAA prediction, which should be further investigated. Next step will be to launch the LBM simulation of a low-noise geometry designed by ONERA, consisting in a 3D morphing of reference airfoils with suited leading-edge serrations, briefly presented in the last section of the paper.

Acknowledgements

The presented work was conducted through a collaboration within the CleanSky2 project InnoSTAT (865007) and has received fundings from European Union's Horizon 2020 research and innovation program in the frame of ADEC project of CS2 LPA-IADP.

References

- [1] Polacsek, C.; Cader, A.; Buszyk, M.; Barrier, R.; Gea-Aguilera, F.; Posson, H. Aeroacoustic Design and Broadband Noise Predictions of a Fan Stage with Serrated Outlet Guide Vanes. *Physics of Fluids*, volume 32, 2020.
- [2] Buszyk, M.; Polacsek, C.; Le Garrec, T. Assessment of a CAA methodology for turbulence cascade interaction noise prediction and reduction from serrated airfoil. *e-Forum Acusticum 2020*, Lyon, France, Decembre 7-11, 2020, pp.2961-2968.
- [3] Buszyk, M.; Polacsek, C.; Le Garrec, T.; Barrier, R.; Bailly, C. 3D CAA methodology using synthetic turbulence to assess turbulence-cascade interaction noise emission and reduction from serrated airfoils. *2021 AIAA Aviation Forum*, 2021.
- [4] Casalino, D.; Avallone, F.; Gonzalez-Martino, I.; Ragni, D. Aeroacoustic study of a wavy stator leading edge in a realistic fan/OGV stage. *Journal of Sound and Vibration*, volume 442, 2019.
- [5] Teruna, C.; Ragni, D.; Avallone, F.; Casalino, D. A rod-linear cascade model for emulating rotor-stator interaction noise in turbofans: A numerical study. *Aerospace Science and Technology*, volume 90, 2019, pp.275-288.
- [6] Teruna, C.; Avallone, F.; Casalino, D.; Ragni, D. Numerical investigation of leading edge noise reduction on a rod-airfoil configuration using porous materials and serrations. *Journal of Sound and Vibration*, volume 494, 2021.
- [7] Clair, V.; Polacsek, C.; Le Garrec, T.; Reboul, G.; Gruber, M.; Joseph, P. Experimental and Numerical Investigation of Turbulence-Airfoil Noise Reduction Using Wavy Edges. *AIAA Journal*, Vol. 51, 2013, pp. 2695–2713.
- [8] Hainaut, T.; Le Garrec, T.; Polacsek, C.; Mincu, D.; Deck, S. Aerodynamic and Aeroacoustic Numerical Investigation of an Axial Fan using Lattice Boltzmann Methods. *2018 AIAA/CEAS Aeroacoustics Conference*, Atlanta, Georgia, June 25-29, 2018.
- [9] Finez, A.; Jondeau, E.; Roger, M.; Jacob, M., "Experimental Investigation of Trailing-Edge Noise from a Linear Cascade of Cambered Airfoils". *7th AIAA/CEAS Aeroacoustics Conference*, Portland, Oregon, June 5-8, 2011.
- [10] Bampanis, G.; Roger, M.; Ragni, D.; Avallone, F.; Teuna, C. Airfoil-Turbulence Interaction Noise Source Identification and its Reduction by Means of Leading Edge Serrations. *25th AIAA/CEAS Aeroacoustics Conference*, Delft, The Netherlands, May 20-23, 2019.
- [11] Jacob, J.; Malaspinas, O.; Sagaut, P. A new hybrid recursive regularised Bhatnagar--Gross--Krook collision model for Lattice Boltzmann method-based large eddy simulation. *Journal of Turbulence*, 2018, pp.1-26.
- [12] Lévêque, E.; Toschi, F.; Shao, L.; and Bertoglio; J. P. Shear-improved Smagorinsky model for large-eddy simulation of wall-bounded turbulent flows. *Journal of Fluid Mechanics*, Vol. 570, 2007, pp. 491–502.